OATAO
Open Archive Toulouse Archive Ouverte

A model of bubble-induced turbulence based on large-scale wake interactions

Guillaume Riboux[1,2], Dominique Legendre[1] and Frédéric Risso[1,†]

[1]Institut de Mécanique des Fluides de Toulouse, CNRS & Université de Toulouse, Allée Camille Soula, 31400 Toulouse, France

[2]Escuela Técnica Superior de Ingenieros, Universidad de Sevilla, Av. de los Descubrimientos s/n, 41092 Sevilla, Spain

Navier–Stokes simulations of the agitation generated by a homogeneous swarm of high-Reynolds-number rising bubbles are performed. The bubbles are modelled by fixed momentum sources of finite size randomly distributed in a uniform flow. The mesh grid is regular with a spacing close to the bubble size. This allows us to simulate a swarm of a few thousand bubbles in a computational domain of a hundred bubble diameters, which corresponds to a gas volume fraction α from $0.6\,\%$ to $4\,\%$. The small-scale disturbances close to the bubbles are not resolved but the wakes are correctly described from a distance of a few diameters. This simple model reproduces well all the statistical properties of the vertical velocity fluctuations measured in previous experiments: scaling as $\alpha^{0.4}$, self-similar probability density functions and power spectral density including a subrange evolving as the power -3 of the wavenumber k. It can therefore be concluded that bubble-induced agitation mainly results from wake interactions. Considering the flow in a frame that is fixed relative to the bubbles, the combined use of both time and spatial averaging makes it possible to distinguish two contributions to the liquid fluctuations. The first is the spatial fluctuations that are the consequence of the bubble mean wakes. The second corresponds to the temporal fluctuations that are the result of the development of a flow instability. Note that the latter is not due to the destabilization of individual bubble wakes, since a computation with a single bubble leads to a steady flow. It is a collective instability of the randomly distributed bubble wakes. The spectrum of the time fluctuations shows a peak around a frequency f_{cwi}, which is independent of α. From the present results it is possible to determine the origin of the overall properties of the total fluctuations observed in the experiments. The scaling of the velocity fluctuation as $\alpha^{0.4}$ is a combination of the scalings of the spatial and temporal fluctuations, which are different from each other. As the time fluctuations are symmetric in the vertical direction, the asymmetry of the probability density function of the vertical velocity comes from that of the spatial fluctuations. Both contributions exhibit a k^{-3} spectral behaviour around the same range of wavenumbers, which explains why it is observed regardless of the nature of the dominant contribution.

Key words: instability, multiphase flow, wakes/jets

1. Introduction

Owing to their rising motion under the action of buoyancy, bubbles immersed in liquid generate an agitation which is sometimes called *pseudo-turbulence*, because it shares some properties with shear-induced turbulence, such as its random character, but also has specific properties, in particular concerning the distribution of energy over the wavelengths. Because of the great number of engineering applications involving bubbly flows, many works have been devoted to the study of pseudo-turbulence. It now appears clear that, depending on the flow configuration, different physical mechanisms are involved. It is indeed essential to differentiate the generation of liquid agitation by the bubble motions from the modulation of shear-induced turbulence by the bubbles (Lance & Bataille 1991). It is also important to distinguish between low-, moderate- and high-Reynolds-number cases (Cartellier & Rivière 2001).

The present work focuses on the agitation generated by bubbles rising at Reynolds numbers Re of order 100–1000, typically corresponding to millimetre-size air bubbles in water. An homogeneous swarm of bubbles rising in a liquid otherwise at rest is very well suited to the study of this phenomenon. In recent years, several experimental works have investigated this configuration (Martinez-Mercado, Palacios-Morales & Zenit 2007; Roig & Larue de Tournemine 2007; Risso *et al.* 2008; Martinez-Mercado *et al.* 2010; Riboux, Risso & Legendre 2010) and determined the main properties of the bubble-induced liquid agitation for various bubble equivalent diameters d and gas volume fractions α. Let us summarize them. Each bubble is followed by a short wake that is considerably shorter than that of a single rising bubble owing to the interaction with the wakes of the surrounding bubbles. The velocity fluctuations scale as $\alpha^{0.4}$. They are anisotropic, large vertical upward fluctuations being more probable that large downward fluctuations. Their probability density functions (p.d.f.s) remain self-similar as α is increased. Their integral length scale is $\Lambda = d/C_d$, where C_d is the bubble drag coefficient. The energy spectrum exhibits a k^{-3} subrange from wavelengths smaller than Λ.

Several direct numerical simulations (DNS) of a swarm of rising bubbles have also been carried out. However, individual bubble dynamics at large Reynolds number is controlled by the vorticity produced at the bubble surface, and its interaction with the bubble wake is responsible for the zig-zag or helicoidal path (Mougin & Magnaudet 2007) and bubble migration (Adoua, Legendre & Magnaudet 2009). Interfacial vorticity is confined in a boundary layer of size $\delta/d \approx Re^{-1/2}$. Typically for the bubble size considered in the experimental studies mentioned above ($d \sim 2$ mm, $Re \sim 800$), the grid spacing for accurate DNS has to satisfy $\Delta/d \sim 0.01$. Owing to the present limitations of computers, predictive DNS of bubbly flows, i.e. with a significant number of bubbles in a domain large enough to make possible the development of the integral length scale of the pseudo-turbulence, are only accessible for grid spacing $\Delta = O(d)$ corresponding to small to moderate bubble Reynolds numbers. Indeed, DNS of bubbly flows are often limited to moderate bubble Reynolds numbers ($Re_b = O(10$–$100)$) for spherical bubbles (Bunner & Tryggvason 2002*a*,*b*; Yin & Koch 2008), nearly spherical bubbles (Esmaeeli & Tryggvason 2005) or ellipsoidal bubbles (Bunner & Tryggvason 2003). Recently, a Reynolds number of order 1000 was reached by Roghair *et al.* (2011) who simulated 16 rising bubbles. With 20 Eulerian mesh points on a bubble diameter, they managed to reproduce experimental p.d.f.s and a k^{-3} spectral range.

Despite the relatively detailed description of the statistical properties of the bubble-induced turbulence that has been achieved, the physics is still obscure. Risso *et al.* (2008) have proposed a reason for that. The liquid fluctuations induced by the bubbles

involve two contributions of different natures. The first contribution is related to the spatial variations of the velocity and called *spatial fluctuation*. Let us assume that all bubbles rise at the same velocity and generate a steady disturbance in the liquid. In the frame that moves at the bubble velocity, the flow is laminar and steady. However, random velocity fluctuations are observed in the laboratory frame. They are simply due to the spatial inhomogeneity of the flow around the bubbles and have nothing to do with turbulence. Under a few elementary conditions, Risso (2011) showed that a superposition of independent random bubble disturbances may generate a continuous spectrum with a k^{-3} subrange. The second contribution corresponds to the genuine temporal fluctuations that develop when the flow becomes unstable at large Reynolds number. It is named *temporal fluctuation*. The understanding of bubble-induced turbulence would benefit greatly if these two contributions could be separated. However, such a decomposition is difficult to achieve in practical situations since bubbles do not rise at constant velocity and move relative to each others. Risso *et al.* (2008) showed that it can however be accomplished by performing spatial and temporal averaging of the flow through a fixed array of obstacles. In their case, they consider an experimental arrangement of solid spheres randomly distributed within a uniform water flow. In the present work, we will present numerical simulations of the flow through a random array of fixed bubbles.

Several experimental results – such as the small contribution of the potential flow to the fluctuating energy, the wake attenuation and the scaling of the integral length scale – make us think that bubble-induced agitation mainly results from wake interactions. We thus propose a simple numerical experiment that consists of assuming that both (i) the motions of the bubbles relative to each other, and (ii) the flow variations at scales smaller than the bubbles, can be neglected. Each bubble is modelled by a fixed source of momentum distributed over a few mesh elements. The flow through a random array of such bubbles is computed by solving Navier–Stokes equations on a mesh grid size of the same order as the bubble diameter. These large-scale simulations allow us to overcome the limitations of DNS and to consider thousands of bubbles in a computational domain of about a hundred bubble diameters, which corresponds to a gas volume fraction α from 0.6 % to 4 %.

The article is organized as follows. Section 2 details the numerical model for both a single bubble and a bubble swarm, and shows validations against experimental results reported by Ellingsen & Risso (2001) and Riboux *et al.* (2010) for a bubble of diameter 2.5 mm rising in water. Section 3 presents results for three different diameters and compares them to experiments by Riboux *et al.* (2010). Section 4 is devoted to the analysis and the discussion of the results from the decomposition of the liquid fluctuation into *spatial* and *temporal fluctuations*. Section 6 summarizes the main conclusions.

2. Model based on large-scale wake interactions

2.1. *Model for an individual bubble wake*

At large distance z downstream of a body, the wake is known to be proportional to the drag experienced by the body, to decay as z^{-1} and to experience a lateral expansion that exponentially decreases with the body Reynolds number (Batchelor 1967). A wake is thus controlled by two main parameters, the Reynolds number based on a characteristic length scale of the body and its drag force. From the observation of bubbles rising in a liquid, the wake development is also affected by the oscillation of the bubble path (Prosperetti *et al.* 2003). As shown by Ellingsen
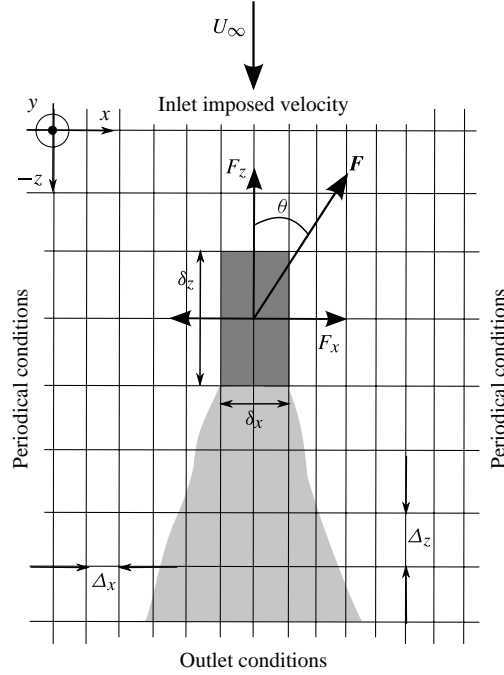
FIGURE 1. Model description and parameter definition.

& Risso (2001) thanks to accurate bubble trajectory reconstruction, the rising velocity of a spheroidal bubble is almost aligned with its small axis and performs vertical oscillations characterized by a maximal inclination θ and a frequency f.

The objective of this section is to propose a simple model able to describe the main characteristics of the wake of a bubble of equivalent diameter $d = 2r$ rising at its vertical terminal velocity V. The model is defined with respect to the bubble Reynolds number, the drag coefficient and the oscillation frequency of the wake. One of our goals is to minimize the cost of the simulations. For this purpose, the flow near each bubble is not resolved as it is the case in DNS, our objective being to correctly reproduce the wake only some distance from of the bubble. This strategy makes accessible simulations for large bubble Reynolds numbers by choosing a grid spacing of the same order of magnitude as the bubble size. The wake is generated by imposing a localized momentum forcing $\boldsymbol{F}$ with components

$$F_x = F_{h0} \cos(\phi) \sin(2\pi f t + \psi), \tag{2.1a}$$

$$F_y = F_{h0} \sin(\phi) \sin(2\pi f t + \psi), \tag{2.1b}$$

$$F_z = F_{z0}, \tag{2.1c}$$

within a uniform flow, $\boldsymbol{U}_\infty = -V\boldsymbol{e}_z$, opposite to the mean vertical bubble velocity. $\boldsymbol{F}$ is uniformly distributed over the volume $\delta_x \delta_y \delta_z$ where δ_x, δ_y and δ_z are the size of the forcing along the x-, y- and z-directions respectively. We denote $\boldsymbol{f} = \boldsymbol{F}/\delta_x \delta_y \delta_z$ the forcing distribution per unit volume. As shown in figure 1, the volume of forcing is distributed over a small number of grid cells N_x, N_y and N_z. F_{z0} is the vertical force component exerted by the body on the fluid along the z-direction and is linked to the

d (mm)	V (cm s^{-1})	f (Hz)	Re (—)	C_d (—)	St (—)	θ (deg.)	$\Lambda = d/C_d$ (mm)
1.6^a	33.5	0	540	0.19	0	0	8.4
2.1^a	32.0	4.6	670	0.27	0.030	25	7.8
2.5^a	30.5	6.3	760	0.35	0.041	28	7.1
2.5^b	30.9	5.0	770	0.34	0.051	25	7.4

TABLE 1. Characteristics of a single air bubble rising in a water. $d = (6\vartheta/\pi)^{1/3}$, bubble equivalent diameter (ϑ is the bubble volume); V average bubble vertical velocity; f, path oscillation frequency; θ maximal inclination of the bubble velocity; $Re = \rho\, dV/\mu$, Reynolds number (ρ and μ are the liquid density and viscosity); $St = f\, d/V$, Strouhal number; C_d, drag coefficient. Λ, integral length scale. ^{a} Riboux *et al.* (2010), ^{b} Ellingsen & Risso (2001).

drag coefficient by:

$$C_d = \frac{2F_{z0}}{\rho\, V^2\, \pi d^2/4}. \tag{2.2}$$

The horizontal forcing F_{h0} is deduced from the vertical drag knowing the maximum angle of oscillation when rising, θ,

$$F_{h0} = \tan(\theta)F_{z0}. \tag{2.3}$$

The vertical plane of oscillation is given by the angle ϕ while ψ is the initial phase of oscillation. Finally, the wake oscillation is characterized by the Strouhal number defined as $St = fd/V$.

Below, the model predictions will be compared with single-bubble experiments by Ellingsen & Risso (2001) and Riboux *et al.* (2010). The corresponding values of Re, C_d, St and θ are given in table 1.

2.2. *Numerical solver*

We solve numerically the incompressible Navier–Stokes equations for the velocity, U, and pressure fields, p,

$$\nabla \cdot U = 0, \tag{2.4}$$

$$\rho\left(\frac{\partial U}{\partial t} + U \cdot \nabla U\right) = -\nabla p + \mu\nabla^2 U + f, \tag{2.5}$$

where ρ is the fluid density and μ its dynamic viscosity. Associated with (2.5) is the volumetric momentum forcing f defined by (2.1), which models the forces exerted by the bubbles.

The computations reported in this paper were carried out with the JADIM code that has been already described in detail in previous studies (Magnaudet, Rivero & Fabre 1995; Legendre & Magnaudet 1998). Briefly, the Navier–Stokes equations written in velocity–pressure variables in a general system of orthogonal curvilinear coordinates are solved here on a regular Cartesian grid. The discretization makes use of a staggered grid on which the equations are integrated in space using a finite-volume method with second-order accuracy. The advection and viscous terms are evaluated through second-order centred schemes whereas time advancement is achieved through a second-order time-accurate Runge–Kutta/Crank–Nicolson algorithm. Finally,

incompressibility is satisfied at the end of each time step by solving a Poisson equation for an auxiliary potential.

Several preliminary simulations (not reported here but presented in Riboux 2007) have been performed in order to test the various numerical parameters of the momentum forcing. Various volumes of forcing with different shapes or involving different numbers of nodes in the vertical and the horizontal directions have been tested. The simulations reveal that the most efficient way to reproduce the velocity defect behind the forcing volume is obtained by distributing the forcing within 8 grid cells, as shown in figure 1, so that $\Delta_z = 2\Delta_x = 2\Delta_y$. The characteristic length scale of the forcing is denoted δ and defined as: $\delta = \Delta_z$.

For most of the simulations reported in this study, the size of the domain is $N_x \times N_y \times N_z = 64 \times 64 \times 128$. This reference mesh grid is referred to as GRID_1 in the following. The time step imposed for all the simulation is $\Delta t = 0.1\delta/V$. The transient evolution of the solution is not considered here and we only focus on results once the flow is established.

In what follows, in order to facilitate the comparison with the experiments, we will present the liquid velocity $\boldsymbol{u}$ in a frame where the bubbles are rising: $\boldsymbol{u} = \boldsymbol{U} + V\,\boldsymbol{e}_z$.

2.3. *Validation for a single bubble*

With the above definition of our model, the relation between the characteristic length δ of the forcing volume and the bubble equivalent diameter d is *a priori* unknown. It is obtained by comparing the simulated evolution of the velocity downstream of the bubble to the measurements obtained by Ellingsen & Risso (2001) for an air bubble of diameter $d = 2.5$ mm rising in water (cf. table 1). The forcing is located in the middle of the domain in the horizontal plane and at $z = -20\Delta_z$ from the inlet, where a uniform velocity is imposed. An outlet condition is imposed at the bottom of the domain and periodic conditions are imposed on the lateral sides of the domain.

Figure 2 reports the evolution with the vertical distance to the bubble centre of the maximal vertical and horizontal velocities normalized by V. The effect of the inclination angle θ is also reported. The best agreement between numerical and experimental results is found for $\delta = d/1.52$. This value, which is consistent with our objective of having a grid spacing of the same order as the bubble diameter, allows the simulation to reproduce well the experimental vertical velocity after a few diameters downstream of the bubble (figure 2a). We also observe that the value of θ has a negligible effect on the vertical velocity whereas it has a very strong effect on the horizontal one (figure 2b). Indeed, with $\theta = 0°$, no horizontal motion is produced. For the value $\theta = 25°$ that corresponds to the vertical inclination of the bubble in the experiments, the magnitude of the horizontal velocity is not correctly reproduced, a larger value for θ being required to observe a satisfactory level.

Figure 3 shows an example of instantaneous velocity field generated by the momentum forcing (2.1) for $Re = 760$, $C_d = 0.35$, $St = 0.05$ and $\theta = 25°$. The case without horizontal forcing is also shown for comparison. Although the computed wake is steady and stable for $\theta = 0°$, the introduction of periodic horizontal forcing makes possible the production of an alternating vortex street.

Results of the model for three bubble diameters listed in table 1 are reported in figure 4. No experiment is available to determine the value of δ for diameters $d = 1.6$ mm and $d = 2.1$ mm. The value $\delta = d/1.52$, which has been determined for $d = 2.5$ mm, is used in all cases. As expected the magnitude of the vertical velocity increases with the diameter since the drag force is increased. The same behaviour is observed for the horizontal component of the velocity.
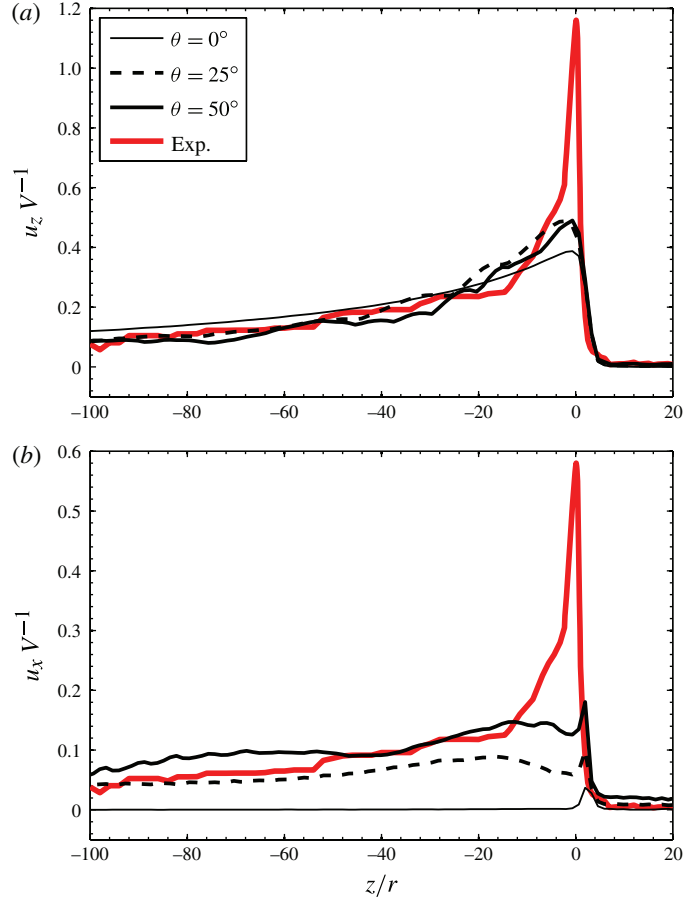
FIGURE 2. (Colour online) Vertical evolution of the vertical (*a*) and horizontal (*b*) velocity in the wake of a single bubble. Numerical results for for $Re = 760$, $C_d = 0.35$, $St = 0.05$ and various values of θ compared with the experiments by Ellingsen & Risso (2001) (thick grey line, red online) for an air bubble of $d = 2.5$ mm rising in water. (Here, $z = 0$ is the bubble location.)

2.4. *Model for the bubble swarm*

Our objective is to determine whether large-scale interactions between wakes are able to reproduce the statistical properties of the bubble-induced turbulence observed in experiments. The bubble swarm is thus modelled by randomly distributing a great number of fixed momentum sources defined by (2.1) within a uniform flow. Except for a minimum distance of 3δ being imposed between two bubbles, the bubble locations are statistically independent from each other. To avoid spurious interactions with the inlet and outlet conditions, the forcing domain starts at $n_{in} = 7\delta$ from the inlet and ends at $n_{out} = 25\delta$ from the outlet. The volume of the forcing domain is thus $\Omega = (N_z - n_{in} - n_{out})N_x N_y \Delta_x \Delta_y \Delta_z$. The gas volume fraction α is calculated from the number N of bubbles inserted in the forcing domain:
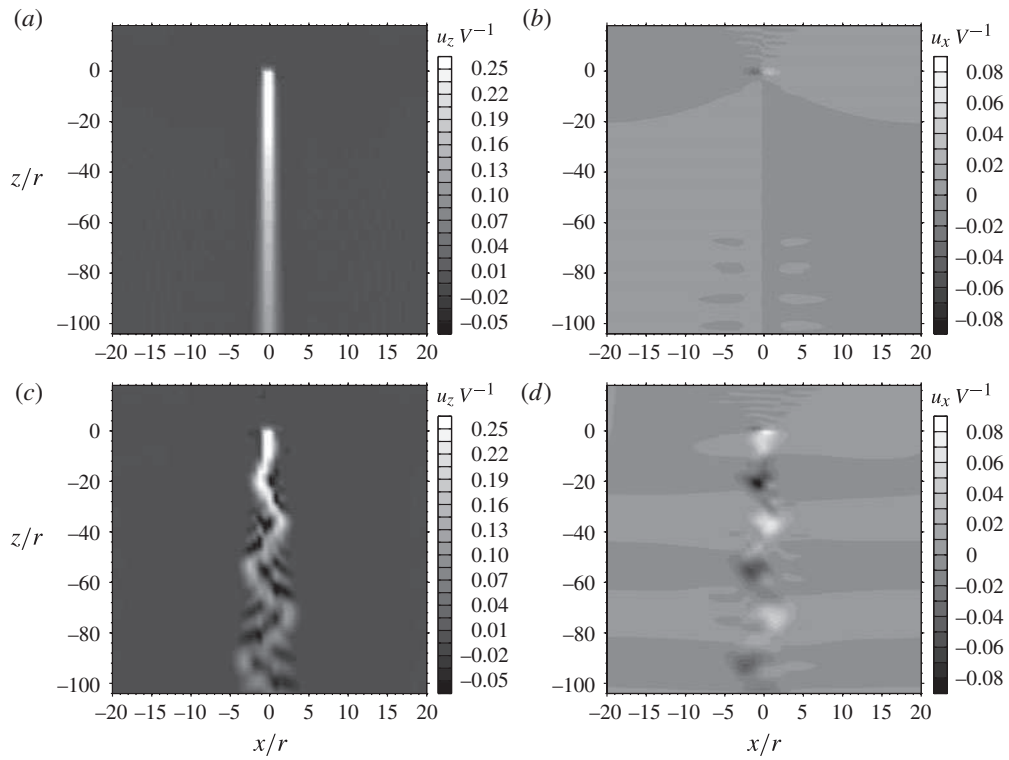
$$N = \frac{6\,\alpha\,\Omega}{\pi\,d^3}. \tag{2.6}$$

FIGURE 3. Instantaneous normalized velocity field for $Re = 760$, $C_d = 0.35$ and $St = 0.05$. (a,b) $\theta = 0°$, (c,d) $\theta = 25°$. (a,c) Vertical component u_z/V, (b,d) horizontal component u_x/V.
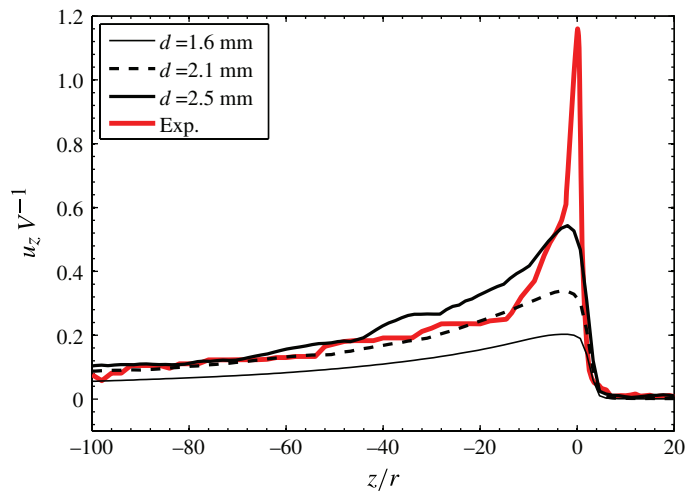

FIGURE 4. (Colour online) Effect of the bubble diameter on the evolution of the vertical velocity in the wake of a single bubble. Exp. denotes the experiments by Ellingsen & Risso (2001) for $d = 2.5$ mm. (Here, $z = 0$ is the bubble location.).
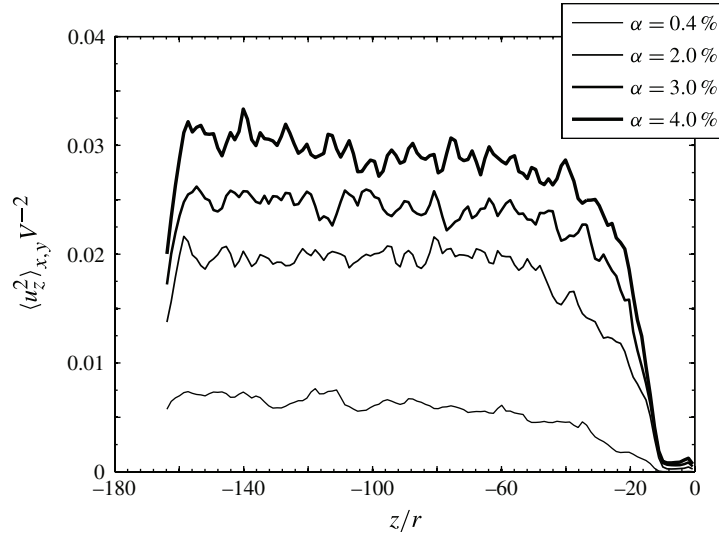
FIGURE 5. Variance of the vertical velocity along the vertical direction for various void fractions (case $d = 2.5$ mm).

The vertical plane of oscillation as well as the temporal phase of oscillation, defined by ϕ and ψ respectively, are also randomly chosen.

In the experiments of Riboux *et al.* (2010), the bubbles were injected by means of capillaries. Owing to this system, the bubble diameters increased as the gas volume fraction was increased. The evolution of the diameter with the void fraction for this set-up was characterized by Colombet *et al.* (2011). Considering the evolutions with the void fraction of both the bubble diameter and the bubble velocity, it turns out that the experiments of Riboux *et al.* (2010) were conducted for an almost constant Reynolds number, $Re = \rho d(\alpha) V(\alpha) / \mu$, and also for an almost constant integral length scale, $\Lambda = d(\alpha)/C_d(\alpha)$. In order to follow the experimental conditions, the present simulations are conducted by keeping constant the values of Re and C_d while changing α for a given value of d. In all simulations, the values of Re and C_d are thus fixed according to the experimental results obtained in a homogeneous bubble swarm.

2.5. *Results and validation for the bubble-swarm model for $d = 2.5$ mm*

In this section, we present simulations of the bubble swarm for the case $d = 2.5$ mm (parameters in table 1), because it is the most documented by Risso & Ellingsen (2002) and Riboux *et al.* (2010) and the one from which the value of δ has been determined.

We first consider the spatial evolution of the fluctuations along the vertical direction through the whole computational domain. Figure 5 shows the evolution of the variance of the vertical fluctuation $\langle u_z^2 \rangle_{x,y}$ averaged in each horizontal plane, for $\theta = 25°$ and various values of α. The energy of the fluctuations first increases rapidly from the beginning of the region where the forcing is applied, then it reaches plateau in the range $-150 \leqslant z/r \leqslant -40$, and finally decreases beyond the end of the forcing region. As expected from a global momentum balance, the pressure gradient is found to be constant in the plateau region and directly proportional to both α and the magnitude of the forcing. We have also checked that the fluctuations are isotropic in
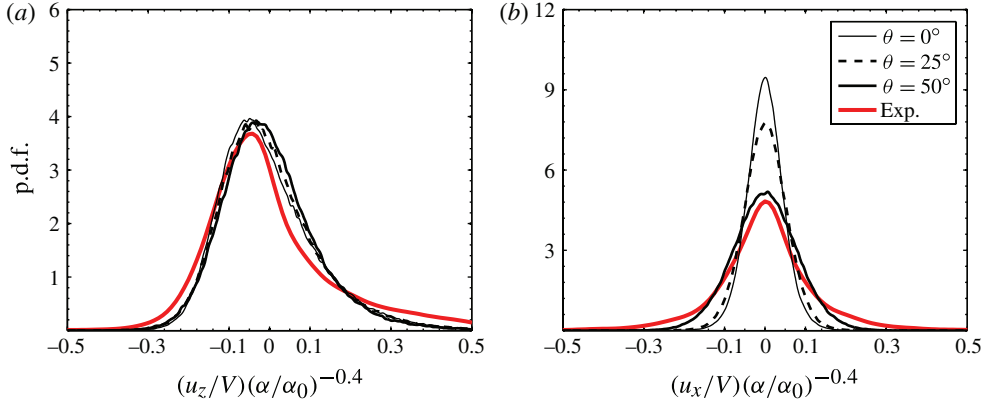
FIGURE 6. (Colour online) Probability density functions (p.d.f.s) for (*a*) the vertical and (*b*) horizontal velocity fluctuations for $d = 2.5$ mm and $\alpha = 2.5\%$ and various horizontal forcings θ. Exp. denotes the experiments by Riboux *et al.* (2010).

the two horizontal directions. In the following all the statistics will be performed for $-150 \leqslant z/r \leqslant -65$ and the two horizontal directions are not distinguished.

The convergence of the simulations toward a statistically steady state has been evaluated by comparing the p.d.f.s of the velocity fluctuations at various times from $t = 20\delta/V$ to $t = 160\,\delta/V$. It turns out that the p.d.f.s are satisfactorily converged after the time $t = 100\,\delta/V$. Hereafter, all presented results have been obtained for $t \geqslant 140\,\delta/V$.

The statistical relevance of the results has been checked by simulating three different bubble swarms, which only differ by the random choice of the bubble locations and the values of ϕ and ψ. The p.d.f.s were found identical for the three cases considered, which ensures that the statistics are converged.

Figure 6 reports the p.d.f.s for the vertical and horizontal velocity fluctuations for $\alpha = 2.5\%$ and various θ. The p.d.f.s of the vertical velocity (figure 6*a*) match very well the experiments. Moreover, as for the case of the single bubble, the vertical fluctuations are not influenced by the periodic horizontal forcing. On the other hand, though the shape of the horizontal p.d.f.s is similar to that of the experiments, their magnitude depends on the horizontal forcing, and it is only for $\theta = 50°$ that the simulated p.d.f.s match the experimental ones.

The one-dimensional average spatial spectrum, S_{zz}, of the vertical fluctuation in the vertical direction is obtained as follows. We consider the profile of the vertical velocity $u_{z,i,j}(z) = u_z(x, y, z)$ at given $x = i\Delta_x$ and $y = j\Delta_y$. We compute the discrete Fourier transform $\widehat{u}_{i,j}(\lambda_z)$ of $u_{z,i,j}(z = k\Delta_z)$. Then S_{zz} is obtained by averaging over the horizontal plane:

$$S_{zz} = \frac{1}{N_i N_j} \sum_i \sum_j |\widehat{u}_{i,j}(\lambda_z)|^2 . \tag{2.7}$$

The one-dimensional average spatial spectrum, S_{xx}, of the horizontal velocity in the horizontal direction is obtained in a similar manner. The discrete Fourier transform $\widehat{u}_{j,k}(\lambda_x)$ is computed from profiles of the horizontal velocity u_x and S_{xx} is obtained by averaging over j and k. Note that S_{yy} has also been computed and is similar to S_{xx}. Figure 7 shows S_{zz} and S_{xx} for $\alpha = 2.5\%$ and various θ. The simulated vertical
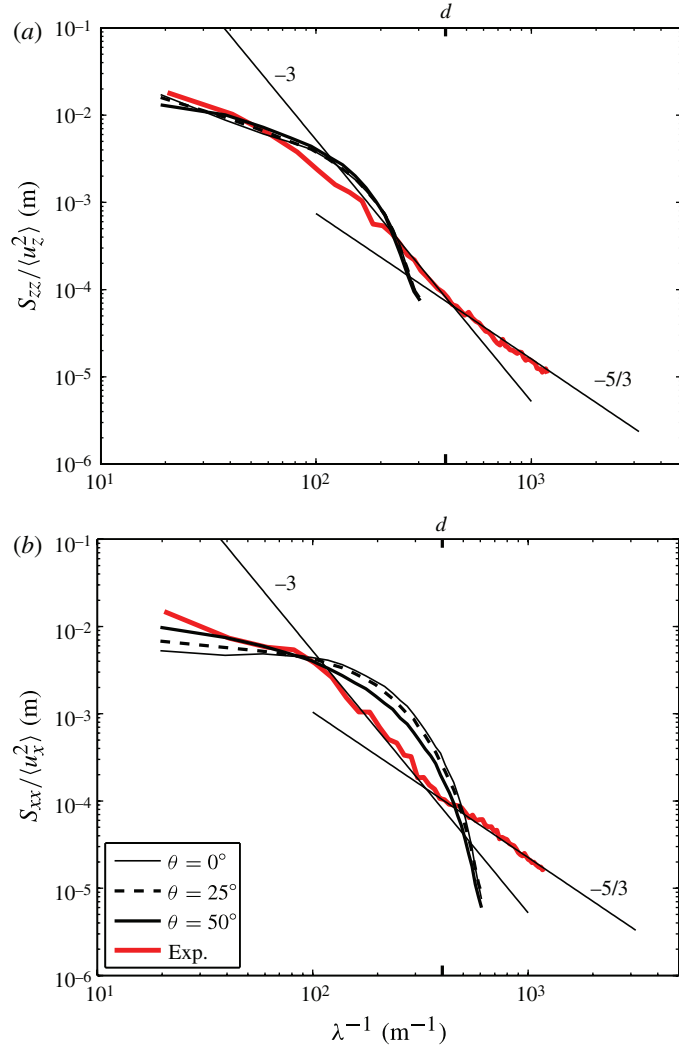
FIGURE 7. (Colour online) (*a*) Vertical and (*b*) horizontal spectra of the liquid velocity fluctuations normalized by their variances for $d = 2.5$ mm, $\alpha = 2.5\%$ and various horizontal forcings θ. Exp. denotes the experiments by Riboux *et al.* (2010).

spectrum matches well the experiments up to the middle of the k^{-3} subrange where it suddenly drops because of the mesh grid limitation. Again, this good agreement at large scales for the vertical fluctuations does not need any horizontal forcing. On the other hand, the simulations are not able to reproduce the spectrum of the horizontal fluctuations. Unlike for the p.d.f.s, increasing θ does not improve the results: it simply increases the energy at large scales but does not generate a k^{-3} subrange. This point will be clarified in § 3.

In order to test the effect of the grid spacing and to extend the spectra to smaller wavelengths, the grid is now refined in the vertical direction so that $N_x \times N_y \times N_z = 64 \times 64 \times 399$. This new grid, referred as GRID$_2$, is regular and the forcing volumes are composed of 16, 4 and 2 cells in the vertical and horizontal
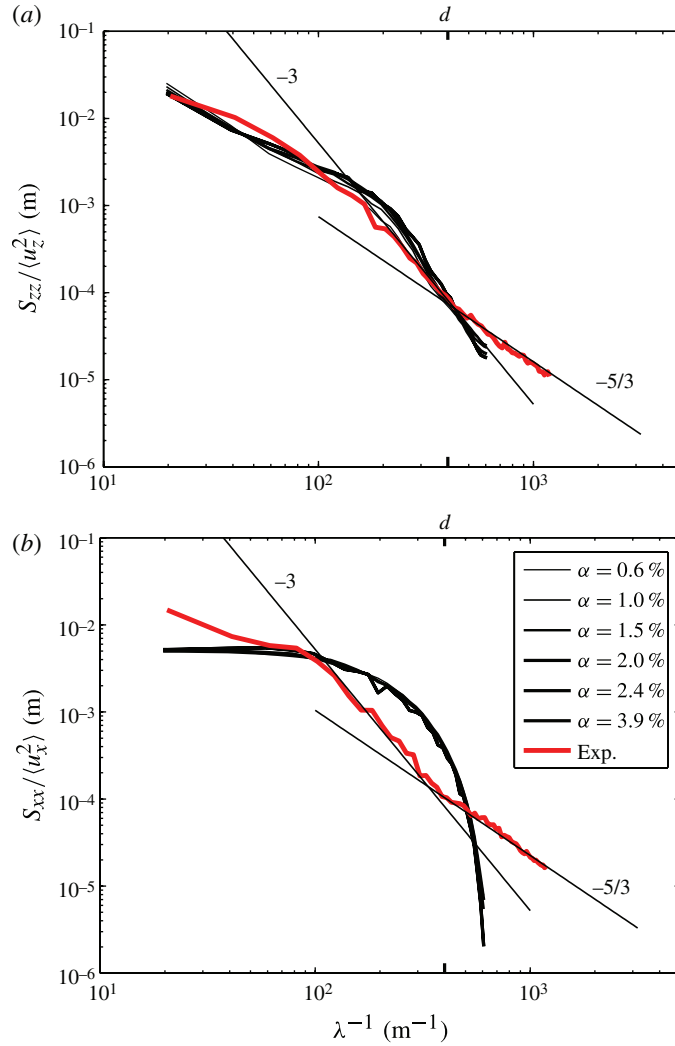
FIGURE 8. (Colour online) Power spectral densities of (*a*) the vertical velocity and (*b*) the horizontal velocity for $d = 2.5$ mm, $\theta = 0°$ and various α for a grid refined in the vertical direction ($N_x \times N_y \times N_z = 64 \times 64 \times 399$). Exp. denotes the experimental spectrum by Riboux *et al.* (2010) for $\alpha = 2.5\%$.

directions, respectively. The corresponding vertical and horizontal spectra are reported in figure 8 for $\theta = 25°$ and various α ranging from 0.6 % to 3.9 %. Concerning S_{zz}, the agreement with the experiment is significantly improved: the k^{-3} subrange starts at $\Lambda \sim d/C_d$ and is observed over almost a decade, until the cutoff imposed by the grid spacing that is now smaller than the bubble size. Concerning S_{xx}, the agreement with the experiments is not improved by the grid refinement in the vertical direction. For both components, it is worth noting that, once normalized by their variance, S_{xx} and S_{zz} are independent of the gas volume fraction, which is in agreement with the experimental observation.

   Let us summarize the conclusions obtained from the comparisons between the present large-scale simulations and previous experiments for the case $d = 2.5$ mm.

(*a*) Concerning the vertical fluctuations, both p.d.f.s and spatial spectra are correctly reproduced without the need of any periodical forcing in the horizontal direction, which anyway has no effect on them.

(*b*) Concerning the horizontal fluctuations, while it is possible to get correct p.d.f.s by using a strong periodical forcing, the spectra are not correctly reproduced whatever the horizontal forcing or the grid refinement.

In the experiments, except for the asymmetry of the vertical fluctuations and differences in magnitude, horizontal and vertical fluctuations have similar properties. This suggests that the same physical mechanisms are acting in both directions. In the present simulations, the horizontal and vertical fluctuations turn out to be independent: while the physical mechanisms seem to be correctly reproduced in the vertical direction, they are not in the horizontal one. This suggests that the momentum source in the direction of the bubble velocity plays a major role in the production of bubble-induced agitation whereas the momentum in the transverse direction has no significant effect. In reality, the direction of the bubble velocity oscillates about the vertical direction. In the simulations, changing the direction of the momentum source is therefore not sufficient; the orientation of the incident flow should also be changed, which is impossible to achieve for each bubble independently.

3. Comparisons with experiments for various bubble diameters

In this section, simulations of the bubble swarm are presented for the three bubble diameters $d = 1.6, 2.1$ and 2.5 mm reported in table 1. They are computed by using the mesh GRID$_1$ and for various gas volume fractions from 0.6 % to 4.3 %.

Figure 9 reports the p.d.f.s of the vertical (*a*) and horizontal (*b*) liquid fluctuations for $\theta = 50°$. The shapes of the p.d.f.s are well reproduced, especially for the case $d = 2.5$ mm. Concerning the vertical p.d.f.s, both the asymmetry and the magnitude are in reasonably good agreement with the experiments. Concerning the horizontal direction, only the case $d = 2.5$ matches the experiments with the chosen of value θ, which confirms that a periodical horizontal forcing does not model correctly the production of agitation in the horizontal direction. For both components, two other important features of the experimental agitation are also well reproduced. First, for a given diameter, the p.d.f.s become independent of the gas volume fraction provided the velocity is normalized by $\alpha^{0.4}$. Second, as revealed on a semi-logarithmic plot (not reported here), the p.d.f.s decrease exponentially as the velocity fluctuation increases.

The vertical spectra, S_{zz}, of the vertical liquid velocity fluctuations computed without any horizontal forcing ($\theta = 0°$) are reported in figure 10. For each of the three diameters considered, the spectra obtained for the different void fractions collapse onto the same curve, provided they are normalized by the variance of the fluctuations. Moreover, the agreement with the experiments of Riboux *et al.* (2010) is very satisfactory. It is remarkable that the simulation not only finds a k^{-3} subrange but also begins at $\Lambda = d/C_d$.

Despite the fact that the value of δ/d (which fixes the length of decay of the wake of an isolated bubble) has only been adjusted for the case $d = 2.5$ mm, the present large-scale simulations are able to reasonably reproduce the p.d.f.s and the spectra of the vertical velocity fluctuations for two other diameters, $d = 1.6$ mm and $d = 2.1$ mm, for gas volume fractions ranging from 0.4 % to 4 %.
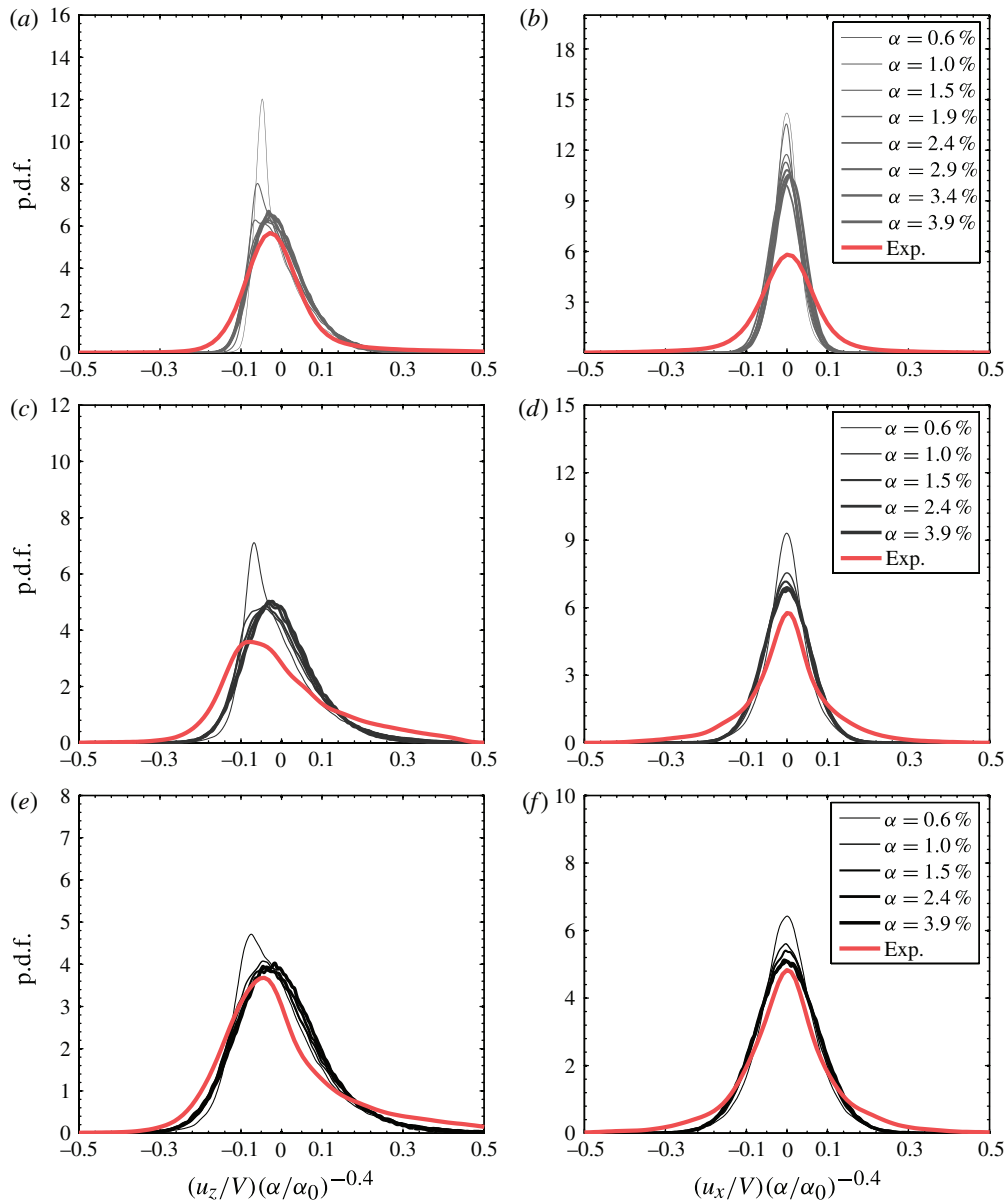
FIGURE 9. (Colour online) p.d.f. of vertical (*a,c,e*) and horizontal (*b,d,f*) liquid fluctuations normalized by $V (\alpha/\alpha_0)^{0.4}$ ($\alpha_0 = 1\%$), for various void fractions ranging from 0.6 % to 3.9 %. Bubble diameters: (*a,b*) $d = 1.6$ mm, (*c,d*) $d = 2.1$ mm, and (*e,f*) $d = 2.5$ mm. In all cases, the horizontal forcing is $\theta = 50°$. Exp. denotes the experimental p.d.f.s by Riboux *et al.* (2010) for $\alpha = 2.5\%$.

4. The dual nature of the bubble-induced turbulence

4.1. *Statistical decomposition of the liquid fluctuations*

The objective of this section is to analyse the bubble-induced agitation by making the distinction between the fluctuations resulting from the local inhomogeneity of the
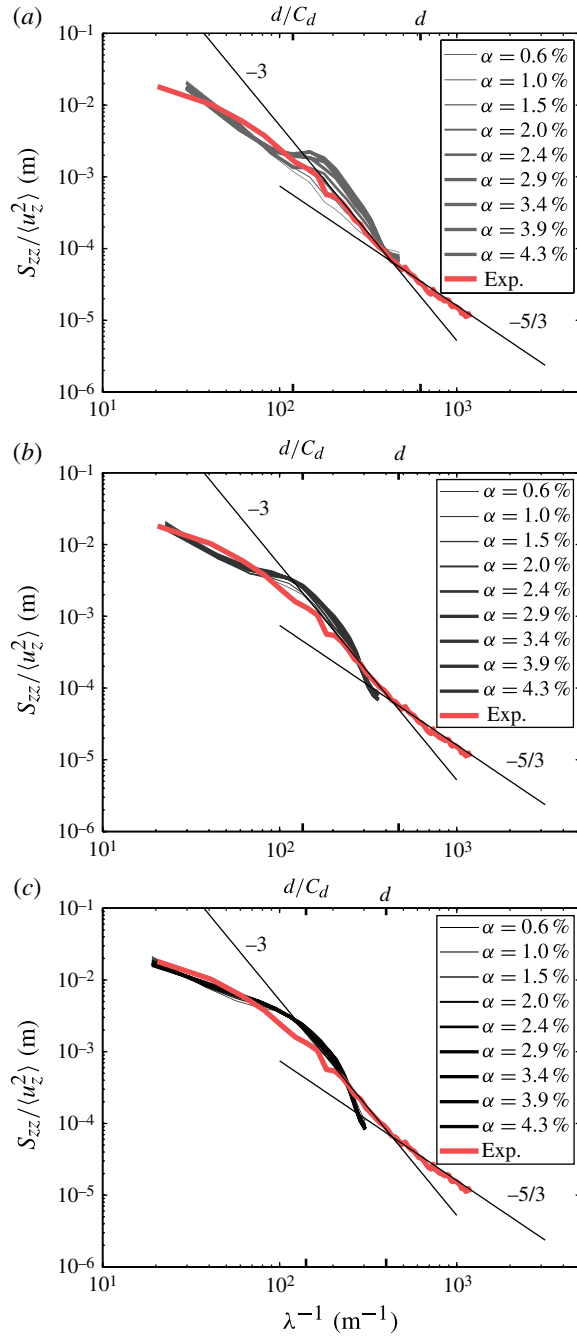
FIGURE 10. (Colour online) Vertical spectra, S_{zz}, of the vertical liquid velocity fluctuation normalized by their variance for various gas volume fractions in the absence of horizontal forcing ($\theta = 0$). Bubble diameters: (a) $d = 1.6$ mm, (b) $d = 2.1$ mm and (c) $d = 2.5$ mm. Exp. denotes the experimental spectra by Riboux et al. (2010) for $\alpha = 2.5\%$.

velocity field and the fluctuations generated by the development of the flow instability. Following Risso *et al.* (2008), we make use of both time averaging (denoted by an overbar), and spatial averaging (denoted by angle brackets, $\langle\ \rangle$). In the frame in which the bubbles are rising, the liquid velocity, $u(x, t) = U(x, t) - U_\infty$, has a zero spatial average. This fluctuation is decomposed as

$$u(x, t) = \overline{u}(x) + u'(x, t). \tag{4.1}$$

The *spatial fluctuation*, $\overline{u}(x)$, is obtained from the time averaging $\overline{u(x, t)}$ of the instantaneous fluctuations and depends only in the position. On the other hand, the *temporal fluctuation*, $u'(x, t)$, depends on both time and space and satisfies $\overline{u'(x, t)} = 0$. The total variance of the velocity fluctuations can thus be decomposed into two contributions

$$\langle u^2 \rangle = \langle \overline{u}^2 \rangle + \langle u'^2 \rangle. \tag{4.2}$$

The simulations are computed by using the mesh GRID_1 over 2000 time steps ($\Delta t = 0.1\,V/d$) before starting the time averaging of the velocity over 3000 time steps. The spatial averaging is made over the central region of the domain where the flow is statistically homogeneous (see §2.5). Since the periodic horizontal forcing fails to model the horizontal fluctuation, θ is set to zero for all the results reported below.

An example of decomposition of the velocity field is shown in figure 11 where $u(x, t)$, $\overline{u}(x)$ and $u'(x, t)$ are reported for $d = 2.5$ mm and $\alpha = 2.5\,\%$ in a vertical plane located in the middle of the domain. The respective contributions of the spatial and temporal fluctuations appear clearly in this figure. Let us consider first the vertical fluctuation (figure 11*a–c*). Mean bubble wakes, which are visible in the total fluctuation, make the major contribution to the spatial fluctuation. On the other hand, the temporal fluctuation turns out to be very little correlated to the bubble wakes and is almost homogeneous over the bubble swarm. An important result is the fact that the flow is unsteady whereas the wake of an isolated bubble computed in the same domain remains perfectly stable and steady during the whole computational time, typically 5000 time steps (see figure 3*a,b*). The time fluctuation therefore results from the development of a flow instability that implies interactions between the wakes of the randomly distributed bubbles. The horizontal fluctuations (figure 11*d–f*) are much lower. The contribution of the mean wakes is negligible, as is the spatial fluctuation. The total fluctuation therefore reduces to the temporal fluctuation, which entirely results from the collective instability of the wakes in the absence of horizontal forcing.

The p.d.f.s of the different contributions to the vertical fluctuations are plotted in figure 12 for $d = 2.5$ and three different volume fractions: $\alpha = 0.6\,\%$ (*a*), $\alpha = 1.5\,\%$ (*b*) and $\alpha = 2.4\,\%$ (*c*). The widths of the p.d.f.s of the spatial and temporal fluctuations are of the same order of magnitude, which indicates that both contribute to the total fluctuation. However, even though the intensity of both contributions increases as α increases, their relative magnitude changes. At $\alpha = 0.6\,\%$, the spatial contribution is clearly dominant and gives the main contribution to the fluctuations. When α is increased, the intensity of the temporal fluctuation increases faster than that of the spatial fluctuation, so that their intensity become comparable at $\alpha = 2.4\,\%$. Figure 12 also reveals that the p.d.f.s of the temporal fluctuation are symmetric whereas those of the spatial fluctuation are asymmetric. The asymmetry of the total fluctuation therefore results from that of the spatial fluctuation, which is the signature of the mean wakes of the bubbles. Since the temporal fluctuation is increasing faster with the gas volume fraction, the asymmetry of the p.d.f. of the total fluctuation is attenuated as α increases. We have also observed that the length of the mean bubble wake, which
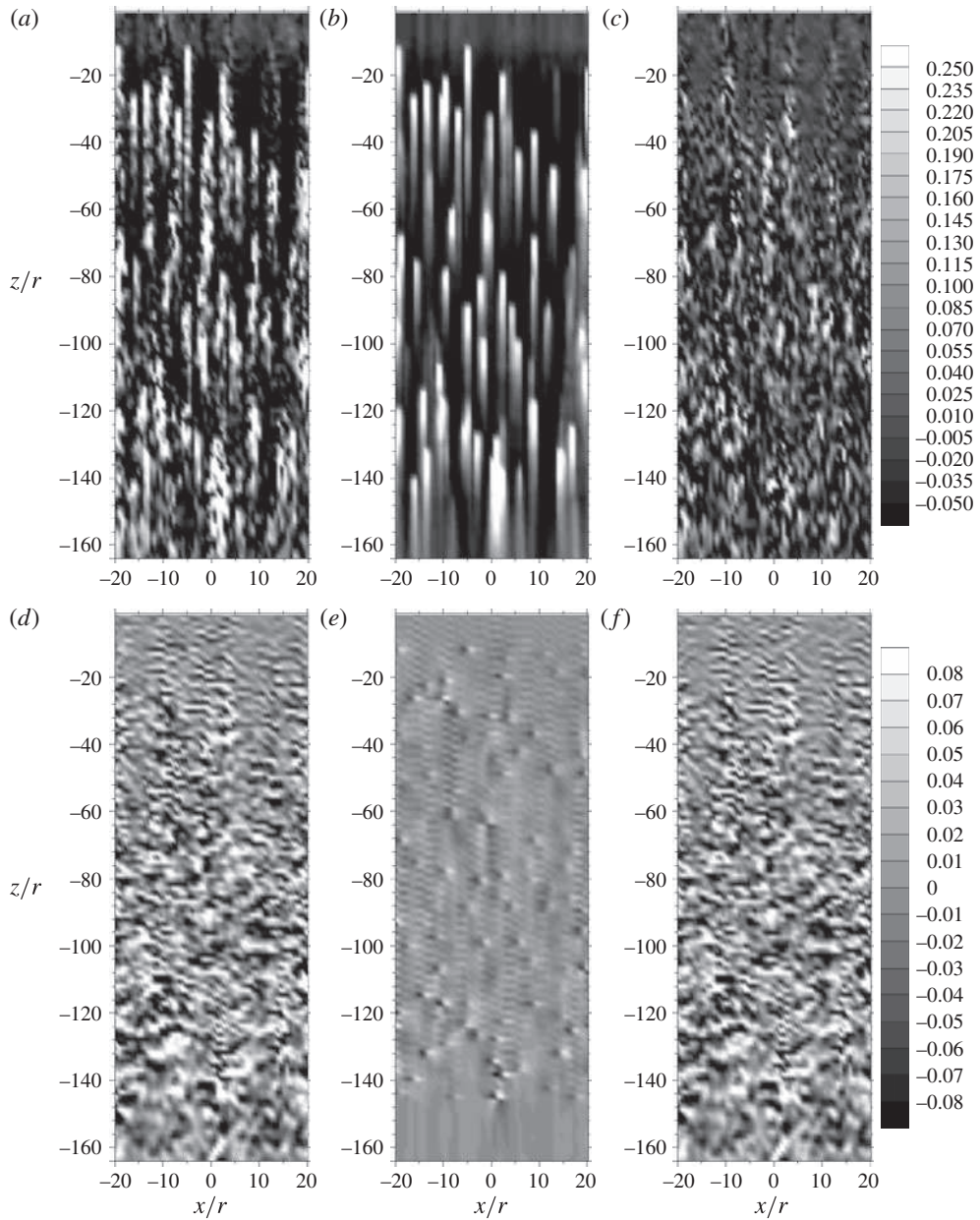
FIGURE 11. Velocity fluctuations normalized by V for $d = 2.5$ mm, $\alpha = 2.5\%$ and $\theta = 0$: (a–c) vertical velocity; (d–f) horizontal velocity. (a,d) Total instantaneous fluctuation $u(x, t)$, (b,e) spatial fluctuation $\bar{u}(x)$ and (c,f) temporal fluctuation $u'(x, t)$.

is visible from the spatial fluctuation in figure 11, decreases with the gas volume fraction. This is consistent with the fact that the wake of a body immersed in ambient turbulence decays faster as the intensity of the turbulence is increased (Wu & Faeth 1995; Bagchi & Balachandar 2004; Legendre, Merle & Magnaudet 2006; Amoura et al. 2010; Botto & Prosperetti 2012). Note that all the conclusions drawn from
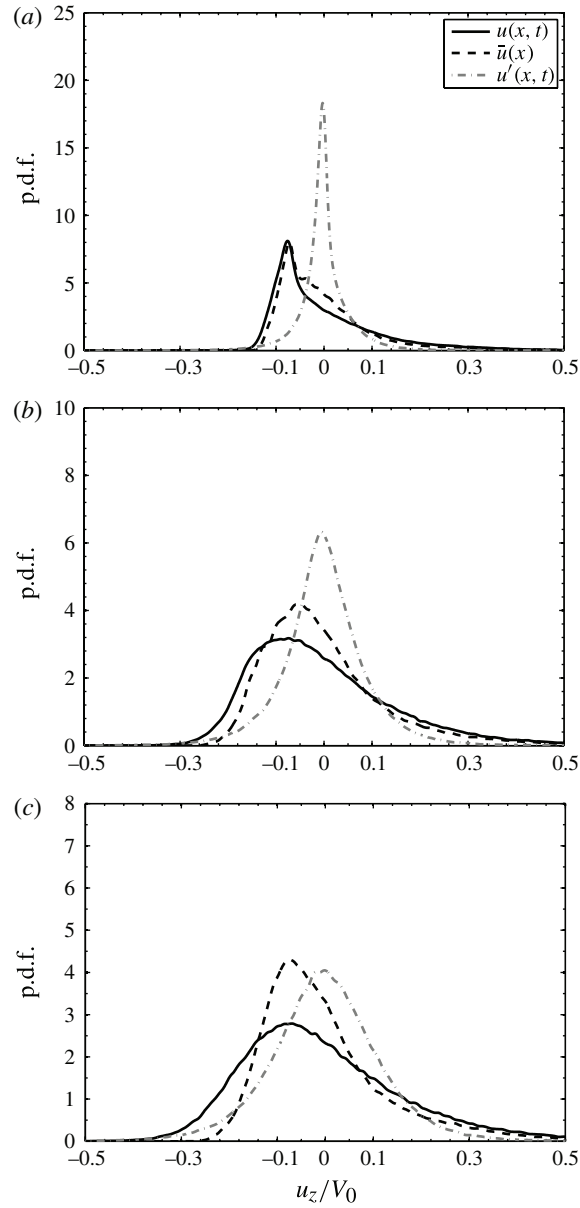
FIGURE 12. Comparison between the p.d.f.s of the spatial and temporal fluctuations for $d = 2.5$ mm for three different gas volume fractions: (a) $\alpha = 0.6\,\%$, (b) $\alpha = 1.5\,\%$ and (c) $\alpha = 2.4\,\%$.

observation of the p.d.f.s of the case $d = 2.5$ remain qualitatively the same for the two other diameters.

The total energy of the fluctuations and the respective contributions of the spatial and temporal fluctuations are shown in figure 13. The three variances are plotted as functions of α for the three diameters. To facilitate the comparison, a logarithmic plot is used and all variances are normalized by the value for the total fluctuation
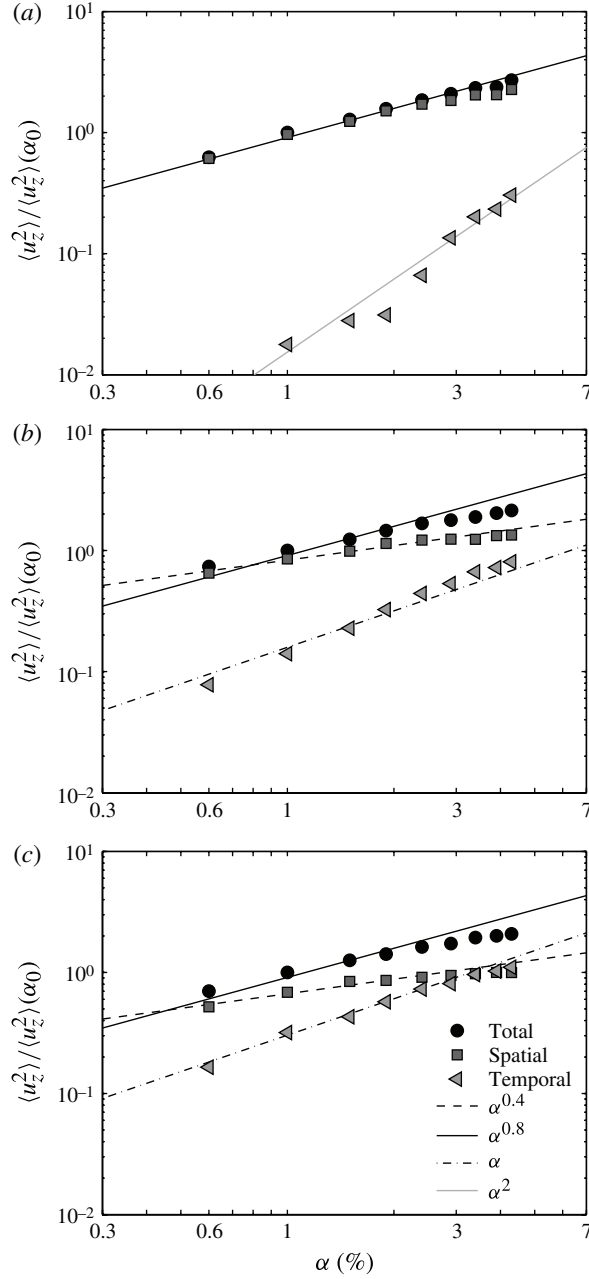
FIGURE 13. Evolution with the gas volume fraction of the variances of the *temporal*, *spatial* and total liquid fluctuations normalized by the variance at $\alpha_0 = 1\%$ ($\theta = 0$). (*a*) $d = 1.6$ mm, (*b*) $d = 2.1$ mm and (*c*) $d = 2.5$ mm. The legends of the three subfigures are the same.

at $\alpha_0 = 1\%$. As expected from the fact that the p.d.f.s of the total fluctuations are self-similar when the velocity is scaled by $V\alpha^{0.4}$ (figure 9), the variance of the total fluctuation broadly evolves as $\alpha^{0.8}$, though a decrease of the slope is visible for the two larger diameters at the largest value of α. However, this exponent is not
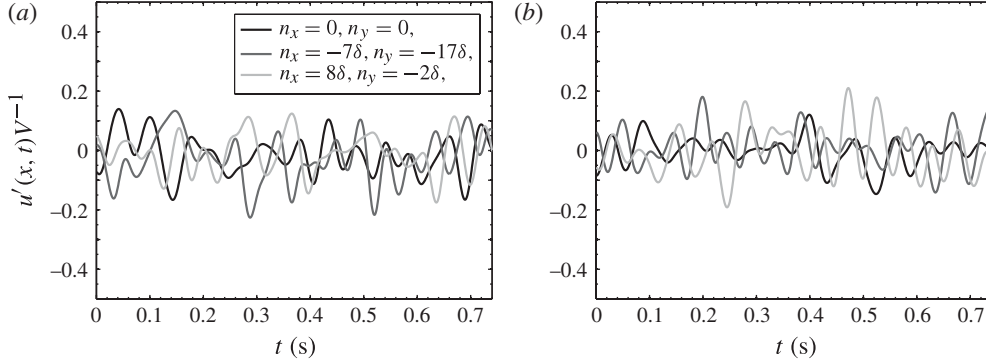
FIGURE 14. Time records of the temporal fluctuation $u'(x,t)$ at three different locations in the domain for $d = 2.5$ mm, $\alpha = 2.5\%$ and $\theta = 0$: (a) vertical velocity and (b) horizontal velocity.

easy to interpret since the total fluctuation is the sum of the spatial and temporal fluctuations, each of which follows its own specific scaling. The smallest diameter case ($d = 1.6$ mm) has a behaviour that differs from the two others. The variance of the temporal fluctuation increases much faster, as α^2, than that of the spatial fluctuation, which evolves as $\alpha^{0.8}$. However, in the considered range of gas volume fractions, the temporal fluctuation remains always negligible and the total fluctuation is almost equal to the spatial fluctuation. When increasing the bubble diameter, the relative importance of the temporal fluctuation increases. A larger Reynolds number and a larger drag coefficient thus seem to favour the development of the flow instability. For $d = 2.1$ mm and $d = 2.5$ mm, the temporal fluctuation evolves as α whereas the spatial fluctuation scales as $\alpha^{0.4}$. Note that it is only for the largest diameter ($d = 2.5$ mm) and the largest volume fractions ($\alpha \approx 4\%$), that the variance of the temporal fluctuation reaches that of the spatial fluctuation.

4.2. Description of the collective wake instability

Time records of the vertical and horizontal temporal fluctuation measured at three different locations within the domain are reported in figure 14 for $d = 2.5$ mm and $\alpha = 2.5\%$. The signals corresponding to the three locations are uncorrelated, which means that the instability does not involve a global fluctuation of the velocity synchronized over the whole domain. The instantaneous fluctuation can reach 20 % of the mean velocity V. Even though the signal is not monochromatic, a dominant frequency seems to emerge from examination of the figure.

The average time spectra of the vertical, S_{zt}, and the horizontal, S_{xt}, fluctuations are computed by averaging the time spectra computed from signals recorded at many locations within the domain. Figure 15 shows S_{zt} and S_{xt} for the three diameters and various gas volume fractions from 0.6 % to 4.3 %. All spectra show a peak at a particular frequency f_{cwi}, which is the frequency at which the energy generated by the collective wake instability is injected into the flow. This frequency is independent of the gas volume fraction and is

$$f_{cwi} = 0.14V/d. \tag{4.3}$$

The peak is very narrow for the smallest diameter ($d = 1.6$ mm) but becomes broader for the two other diameters ($d = 2.1$ mm and $d = 2.5$ mm). The peak is also observed

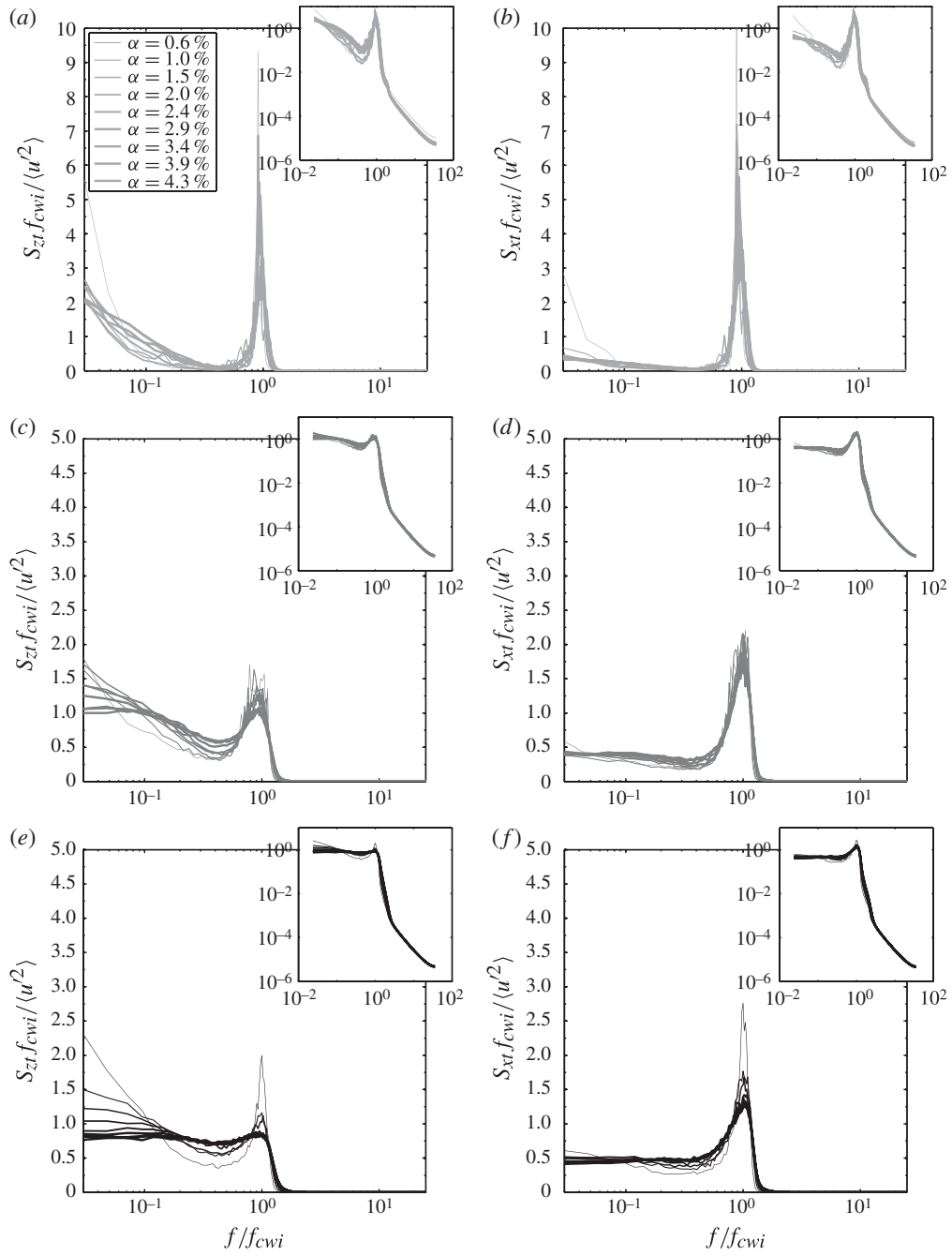FIGURE 15. Time spectra of the temporal fluctuation: (*a,b*) $d = 1.6$ mm, (*c,d*) $d = 2.1$ mm and (*e,f*) $d = 2.5$ mm. (*a,c,e*) Vertical component and (*b,d,f*) horizontal component. The insets show the same plots in logarithmic representation.

to become broader as the volume fraction increases. It thus seems that the peak width is an increasing function of the intensity of the temporal fluctuation. As the instability develops, due to the increase of either the Reynolds number or the number of momentum sources, the range of frequency wherein the energy of the instability is injected spreads more and more. For the largest diameter ($d = 2.5$ mm), the spectrum seems to converge, for sufficiently large volume fractions, towards a master curve, $G(f/f_{cwi})$, that is independent of α. Since the variance of the temporal fluctuation has been shown to be proportional to α, the asymptotic spectrum can be written

$$S_{zt}(f) = \alpha V^2/f_{cwi}G(f/f_{cwi}). \qquad (4.4)$$

4.3. Spacial spectra of temporal and spatial fluctuations

The contributions of the temporal and spatial fluctuations to the spatial spectra, S_{zz} and S_{xx}, are now considered. As for the total fluctuation (figure 8), the spectra of both contributions are also independent of the gas volume fraction when normalized by their variance. Since the evolution of the variances has been already discussed, we will only present the spectra computed for a single volume fraction, $\alpha = 2.4\,\%$. Figure 16 shows the spectra of the vertical and horizontal velocity components for the three diameters.

Let us consider first the vertical velocity (figure 16a,c,e). At $d = 1.6$ mm, the temporal fluctuation shows a peak, indicating that the energy of the instability is preferentially injected into a specific range of wavenumbers as it is injected into a specific range of frequencies. After the peak, the spectrum of the temporal fluctuation decreases as k^{-3} before experiencing a sudden cutoff. On the other hand, the spatial fluctuation shows a more regular evolution not far from a k^{-3} behaviour in the whole investigated range. Comparing both fluctuations, the spatial one is dominant at large and small scales, whereas the temporal one is slightly larger in the region that follows the peak. In the region where the k^{-3} subrange is observed for the total fluctuations, both contribution also follow a k^{-3} evolution. When increasing the diameter, the shape of the spectrum of the spatial fluctuation remains unchanged whereas the peak of the temporal fluctuation disappears. For $d = 2.1$ mm and $d = 2.5$ mm, the relative contribution of the temporal fluctuation becomes predominant on almost the whole range of wavenumbers, especially in the k^{-3} subrange of the total fluctuation. It is only at the very largest scales that the mean bubble wakes can compete with the flow instability. In the horizontal fluctuation (figure 16b,d,f), the footprint of the mean wakes is very small and the temporal fluctuation is the dominant contribution for the whole range of wavenumbers and for the three diameters. Even though we know that the horizontal fluctuations are not correctly reproduced by the present simulations, it is still interesting to note that the spectra of both contributions are close to a k^{-3} behaviour in the expected range of wavenumbers.

The most striking point is that, even though they are totally different phenomena, both the spatial fluctuation and the temporal fluctuation show a k^{-3} subrange. It is therefore not sufficient to observe a k^{-3} subrange in a particular dispersed multiphase flow to know what the dominant contribution is. For the spatial fluctuation, the reason for such a spectral behaviour has been explained by Risso (2011) who demonstrated that a superposition of independent velocity disturbances of random sizes can generate a k^{-3} subrange. Regarding the temporal fluctuation, the k^{-3} subrange is a characteristic of a collective instability of the randomly distributed wakes, which still remains to be understood.
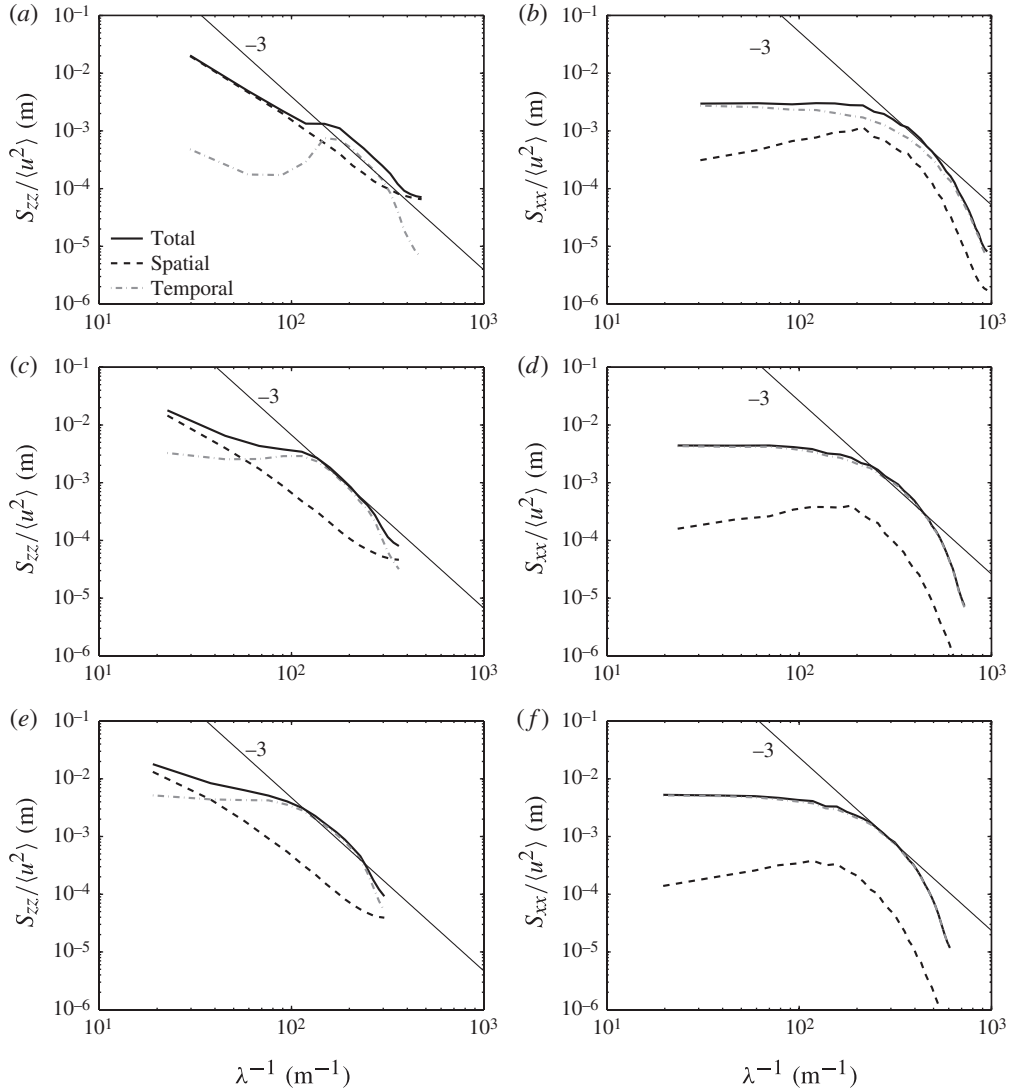
FIGURE 16. Spatial spectra of the vertical component of the fluctuations S_{zz} (a,c,e) and horizontal component of the fluctuations S_{xx} (b,d,f) for $\alpha = 2.4\%$ and the three diameters: (a,b) $d = 1.6$ mm, (c,d) $d = 2.1$ mm and (e,f) $d = 2.5$ mm.

5. *A posteriori* discussion of the model assumptions

The good agreement between the model and the experiments has confirmed our intuition that large-scale wake interactions are predominant in the generation of bubble-induced agitation. Let us recall and discuss the model assumptions.

The bubbles are assumed to be immobile relative to each other. In reality, the bubbles do not have exactly the same average velocity. This causes their spatial distribution to change. The present model is not able to deal with bubbly flows where significant variations of gas volume fractions occur. Since we focus on situations where the bubble distribution remains statistically homogeneous, their relative motions have no significant consequences on the liquid agitation. Also, the bubble paths

oscillate due to wake instability. It turns out that the mechanisms that generate the liquid agitation are independent of the bubble agitation. However, changes in bubble velocity directions probably play a role in the redistribution of the energy between the vertical and the horizontal liquid fluctuations, which cannot be accounted for by an horizontal oscillatory drag.

This model reproduces situations with bubbles that all have the same vertical drag, which is constant with time. Even if the bubbles are not spherical, they keep an almost constant spheroidal shape: shape oscillations therefore do not influence significantly the bubble drag. Concerning polydispersity, we have performed additional simulations in which bubble diameters were randomly distributed in a range of $\pm 2.5\,\%$ around the average value. This had no visible consequence on the statistics of the velocity fluctuations. The present model is therefore robust with regard to a small polydispersity.

Another major assumption of the model is that the scales that are smaller than the bubble diameter do not play a significant role. To discuss this point we need again to distinguish the spatial and temporal fluctuations. The spatial fluctuations result from the local spatial heterogeneity of the average flow disturbance around and behind each bubble. It is therefore expected that most of their energy belongs to scales that are of the same order as, or larger than, the bubble size. The temporal fluctuations turn out not to result from the development of flow instability within individual wakes but from a collective instability of randomly distributed wakes. That probably explains why they can be reproduced by large-scale simulations, provided that the main characteristics of the wakes are well described. The smallest scales possibly play a role in the determination of the precise value of the onset of this instability, but do not have a significant effect on the statistics of the fluctuations when it is developed. Note that for both kinds of fluctuations, the fast decay of the fluctuating energy with the wavenumber, as k^{-3}, reduces the possibility of a feedback from small to large scales.

In order to apply this model to more complex situations, the next step is to allow the bubbles to move. First, we expect that if the bubble velocity direction oscillates around the vertical, realistic horizontal liquid velocity fluctuations should be generated. Second, by implementing a Lagrangian force balance to compute the motion of each bubble, situations with non-uniform gas volume fractions could be investigated.

6. Concluding remarks

We have proposed a model of bubble-induced agitation based on the interactions between bubble wakes at scales larger than the bubble size. Two main assumptions have been made. The first is that flow disturbances generated at scales smaller than the bubble diameter do not play a significant role. The second consists of neglecting bubble velocity fluctuations. The flow through a random array of bubbles has thus been computed by solving the Navier–Stokes equations on a mesh grid with a spacing of the same order as the bubble size, each bubble being modelled by a fixed source of momentum distributed over a volume close to the bubble size.

The results of these large-scale simulations have been compared with previous experimental results obtained for homogeneous swarms of air bubbles rising in water. Three bubble diameters have been considered ($d = 1.6, 2.1$ and 2.5 mm), which correspond to Reynolds numbers between 500 and 800. Gas volume fractions ranging from $0.6\,\%$ to $4\,\%$ have been investigated. The simulations are shown to reproduce remarkably well the statistics of the vertical liquid velocity: variance, probability density functions and spectra. Horizontal velocity fluctuations are however not well

described, probably because velocity fluctuations are essentially generated in the direction of the motion of the bubbles, which is fixed in the simulation while it oscillates in experiments. This effect cannot be accounted for by making the direction of the momentum sources oscillate.

These results lead to the following conclusions. Large-Reynolds-number bubble-induced agitation is mainly caused by large-scale wake interactions. Bubble motions relative to each other can be neglected but bubble velocity oscillations probably play a major role in the distribution of energy between the vertical and the horizontal velocity fluctuations.

Taking advantage of the fact that the bubbles are fixed relative to each other, the fluctuations have been decomposed into a time-averaged *spatial fluctuation* and a genuine *temporal fluctuation*. The spatial fluctuation accounts for the energy of individual bubble mean wakes. The temporal fluctuation is the result of a collective instability of the randomly distributed wakes. This instability is observed to inject energy into the flow around a characteristic frequency f_{cwi}, which is independent of the gas volume fraction and scales as the ratio between the bubble velocity and the bubble diameter. In experiments, the fluctuation that is measured is the sum of the spatial and the temporal fluctuations. Since the evolutions of the energy of the two fluctuations with the gas volume fraction are different, their contribution to the total energy depends on α and the scaling of the total variance is the result of the combination of two different mechanisms. On the other hand, the spectra of both contributions include a k^{-3} subrange. The observation of such a spectral behaviour in the total fluctuations measured in any dispersed two-phase flow is thus not sufficient to draw conclusions about the nature of the dominant contribution. While a theoretical derivation of the k^{-3} subrange has been proposed for the spatial fluctuation (Risso 2011), the mechanism underlying the collective instability of random wakes still needs to be elucidated.

REFERENCES

ADOUA, R., LEGENDRE, D. & MAGNAUDET, J. 2009 Reversal of the lift force on an oblate bubble in a weakly viscous linear shear flow. *J. Fluid Mech.* **628**, 23–41.

AMOURA, Z., ROIG, V., RISSO, F. & BILLET, A.-M 2010 Attenuation of the wake of a sphere in an intense incident turbulence with large length scales. *Phys. Fluids* **22** (5), 008005PHF.

BAGCHI, P. & BALACHANDAR, S. 2004 Response of the wake of an isolated particle to an isotropic turbulent flow. *J. Fluid Mech.* **518**, 95–123.

BATCHELOR, G. K. 1967 *An Introduction to Fluid Dynamics*. Cambridge University Press.

BOTTO, L. & PROSPERETTI, A. 2012 A fully resolved numerical simulation of turbulent flow past one or several spherical particles. *Phys. Fluids* **24** (1), 013303.

BUNNER, B. & TRYGGVASON, G. 2002a Dynamics of homogeneous bubbly flows. Part 1. Rise velocity and microstructure of the bubbles. *J. Fluid Mech.* **466**, 17–52.

BUNNER, B. & TRYGGVASON, G. 2002b Dynamics of homogeneous bubbly flows. Part 2. Velocity fluctuations. *J. Fluid Mech.* **466**, 53–84.

BUNNER, B. & TRYGGVASON, G. 2003 Effect of bubble deformation on the properties of bubbly flows. *J. Fluid Mech.* **495**, 77–118.

CARTELLIER, L. & RIVIÈRE, A. 2001 Bubble-induced agitation and microstructure in uniform bubbly flows at small to moderate particle Reynolds numbers. *Phys. Fluids* **13** (8), 2165–2181.

COLOMBET, D., LEGENDRE, D., COCKX, A., GUIRAUD, P., RISSO, F., DANIEL, C. & GALINAT, S. 2011 Experimental study of mass transfer in a dense bubble swarm. *Chem. Engng Sci.* **66** (14), 3432–3440.

ELLINGSEN, K. & RISSO, F. 2001 On the rise of an ellipsoidal bubble in water: oscillatory paths and liquid-induced velocity. *J. Fluid Mech.* **440**, 235–268.

ESMAEELI, A. & TRYGGVASON, G. 2005 A direct numerical simulation study of the buoyant rise of bubbles at $O(100)$ Reynolds numbers. *Phys. Fluids* **17** (9), 093303.

LANCE, M. & BATAILLE, J. 1991 Turbulence in the liquid phase of a uniform bubbly air–water flow. *J. Fluid Mech.* **222**, 95–118.

LEGENDRE, D. & MAGNAUDET, J. 1998 The lift force on a spherical bubble in a viscous linear shear flow. *J. Fluid Mech.* **368**, 81–126.

LEGENDRE, D., MERLE, A. & MAGNAUDET, J. 2006 Wake of a spherical bubble or a solid sphere set fixed in a turbulent environment. *Phys. Fluids* **18** (4), 048102.

MAGNAUDET, J., RIVERO, M. & FABRE, J. 1995 Accelerated flows past a rigid sphere or a spherical bubble. Part 1. Steady straining flow. *J. Fluid Mech.* **284**, 97–135.

MARTINEZ-MERCADO, J., GÓMEZ, D. C., GILS, D. V., SUN, C. & LOHSE, D. 2010 On bubble clustering and energy spectra in pseudo-turbulence. *J. Fluid Mech.* **650**, 287–306.

MARTINEZ-MERCADO, J., PALACIOS-MORALES, C. & ZENIT, R. 2007 Measurement of pseudoturbulence intensity in monodispersed bubbly liquids for $10 < Re < 500$. *Phys. Fluids* **19** (10), 103302.

MOUGIN, G. & MAGNAUDET, J. 2007 Wake instability of a fixed spheroidal bubble. *J. Fluid Mech.* **572**, 311–337.

PROSPERETTI, A., OHL, C., TIJINK, A., MOUGIN, G. & MAGNAUDET, J. 2003 Leonardo's paradox. *J. Fluid Mech.* **482**, 286–289.

RIBOUX, G. 2007 Hydrodynamique d'un essaim de bulles en ascension. PhD thesis, Institut National Polytechnique de Toulouse.

RIBOUX, G., RISSO, F. & LEGENDRE, D. 2010 Experimental characterization of the agitation generated by bubbles rising at high Reynolds number. *J. Fluid Mech.* **643**, 509–539.

RISSO, F. 2011 Theoretical model for k^{-3} spectra in dispersed multiphase flows. *Phys. Fluids* **23** (1), 011701.

RISSO, F. & ELLINGSEN, K. 2002 Velocity fluctuations in homogeneous dilute dispersion of high-Reynolds-number rising bubbles. *J. Fluid Mech.* **453**, 395–410.

RISSO, F., ROIG, V., AMOURA, Z., RIBOUX, G. & BILLET, A.-M. 2008 Wake attenuation in large Reynolds number dispersed two-phase flows. *Phil. Trans. R. Soc. Lond.* A **366** (1873), 2177–2190.

ROGHAIR, I., MERCADO MARTÍNEZ, J., VAN SINT ANNALAND, M., KUIPERS, H., SUN, C. & LOHSE, D. 2011 Energy spectra and bubble velocity distributions in pseudo-turbulence: numerical simulations versus experiments. *Intl J. Multiphase Flow* **37** (9), 1093–1089.

ROIG, V. & LARUE DE TOURNEMINE, A. 2007 Measurement of interstitial velocity of homogeneous bubbly flows at low to moderate void fraction. *J. Fluid Mech.* **572**, 87–110.

WU, J. S. & FAETH, G. M. 1995 Effect of ambient turbulence intensity on sphere wakes at intermediate Reynolds numbers. *AIAA J.* **33** (1), 171–173.

YIN, X. & KOCH, D. L. 2008 Lattice–Boltzmann simulation of finite Reynolds number buoyancy-driven bubbly flows in periodic and wall-bounded domains. *Phys. Fluids* **20**, 103304.